Hydrodynamic performance of vegetation surrogates in hydraulic studies: a comparative analysis of seaweed blades and their physical models

Hydrodynamic performance of seaweed blades and their surrogates: a comparative analysis

OR

Hydrodynamic performance of vegetation surrogates: a comparative analysis of seaweed blades and their surrogates

DAVIDE VETTORI (IAHR MEMBER), Postdoctoral Research Associate, *Department of Geography, Loughborough University, Epinal Way, Loughborough LE11 3TU, UK.*

Email: d.vettori@lboro.ac.uk (Author for correspondence)

VLADIMIR NIKORA (IAHR Member), Professor, *School of Engineering, University of Aberdeen, Aberdeen AB24 3UE, Scotland, UK.*

Email: v.nikora@abdn.ac.uk

Running Head (i.e. the text that appears in the top margin of the published page):
Hydrodynamic performance of seaweeds and their surrogates.

Hydrodynamic performance of seaweed blades and their surrogates: a comparative analysis

OR

Hydrodynamic performance of vegetation surrogates: a comparative analysis of seaweed blades and their surrogates

ABSTRACT

Artificial surrogates of vegetation have been used extensively in laboratory experiments for studying flow-vegetation interactions. An unaddressed dilemma is if surrogates successfully replicate the performance of prototype vegetation, particularly as in many cases they are not designed within a similarity framework nor considering vegetation biomechanics. In the present study we compare the hydrodynamic performance of seaweed blades of the species *Saccharina latissima* and that of their artificial surrogates which were designed based on bespoke similarity considerations. To assess the hydrodynamic performance of a test sample, we measured flow velocities upstream and downstream of a sample, its vertical movements, and the drag force it experienced. Results reveal that mechanisms governing flow-seaweed blade interactions are the same for live blades and surrogates. Artificial surrogates successfully replicate many aspects of blade dynamics, but underestimate drag force and reconfiguration of live blades likely because of their simplified morphology which lacks macro-features and roughness elements.

Keywords: Drag coefficient; Flow-biota interactions; Hydraulic models; Turbulent wakes; Similarity theory; Velocity measurements

1 Introduction

In the last decades, vegetation has been explored extensively by hydraulic engineers and researchers alike because of its role in governing channel hydraulics, and its impacts on sediment transport and on flood risk. The first pioneering studies with vegetation were conducted by Kouwen *et al*. (1969) and Kouwen and Unny (1973) who examined the impact of vegetation on the roughness parameters used to estimate hydraulic conditions in open channels. Countless studies on flow-vegetation interactions have followed, many of which made use of artificial surrogates (e.g. Wilson *et al.* 2003, Folkard 2005, Albayrak *et al.* 2012, Siniscalchi *et al.* 2012, Rominger and Nepf 2014), which allow a control over experimental conditions not achievable with live vegetation (Frostick *et al*. 2011). Use of vegetation surrogates is particularly attractive in studies at

big spatial scales (e.g. patch, canopy, reach scales) where many elements are required, while it is less common in studies at small spatial scales. For example, rigid cylinders have been used in a number of studies investigating flow within vegetated canopies (e.g. Ghisalberti and Nepf 2005, Lightbody and Nepf 2006), even though representing vegetation using rigid cylinders is not generally justifiable (Aberle and Järvelä 2013).Vegetated beds have also been reproduced using artificial rigid strips (Nezu and Sanjou 2008), artificial garden grass (Nikora *et al.* 2013), and strips prepared from polyethylene sheeting (Folkard 2005). At a smaller scale, Albayrak *et al.* (2012) studied the effects of mechanical properties and morphological characteristics of leaves on flow-vegetation interactions. While in a few studies (e.g. Folkard 2005) surrogate design was based on similarity in geometric properties and mechanical characteristics to prototype vegetation, most research up-to-date has been conducted using vegetation surrogates which were not scaled appropriately.

In recent years the interactions between flow and seaweeds have been studied following the development of multiple potential applications associated with economic and/or environmental benefits (see Lucas and Southgate 2012, for details on applications). Artificial surrogates of seaweeds (or seaweed blades) have been employed by Johnson (2001) and Stewart (2006), who did not consider similarity theory when scaling their samples, and Rominger and Nepf (2014), Fryer *et al*. (2015) and Vettori and Nikora (2017b), who designed and manufactured their surrogates according to a similarity theory that accounts for the most significant parameters in play. These studies have contributed to developing an understanding of how seaweeds interact with the flow at a range of conditions and depending on the morphological characteristics and mechanical properties of the surrogates. To the best of our knowledge, however, the reliability of seaweed surrogates has never been assessed in terms of how well their hydrodynamic performance replicate that of their prototypes. To widen the knowledge gap further, this problem has never been tackled in flow-vegetation interactions studies in general. Yet, this is pivotal to understand the accuracy with which artificial surrogates should be designed.

Whilst in classic hydraulic engineering applications we deal (mainly) with static structures, in studies of flow-vegetation interactions we must account for vegetation reconfiguration where relevant. In cases in which vegetation does not deform or move maintaining geometrical similarity is sufficient. However, these cases are an exception rather than the norm, and most aquatic and riparian vegetation is subjected to reconfiguration at a broad range of hydraulic conditions. On this account, it is important to bear in mind that reconfiguration can be considered as a combination of posture (i.e. static reconfiguration) and motion (i.e. dynamic reconfiguration, *sensu* Siniscalchi and

Nikora 2013). Therefore, an appropriate replica would not only maintain geometric similarity, but it would also behave as the prototype at the relevant range of hydraulic conditions, thus maintaining kinematic and dynamic similarities as well. Unfortunately, maintaining all three similarities in a surrogate is often impracticable, particularly when the surrogate is down-scaled. Nevertheless, design of surrogates should be carried out in a similarity framework by taking into account the most important governing parameters in the prototype (e.g. de Langre 2008, Nikora 2010). This is subordinate to our knowledge of morphological characteristics and mechanical properties of vegetation, an area in which data are eminently needed.

Even though the use of a similarity framework in flow-vegetation interactions studies appears to be spreading in the hydraulic research community, it is currently unclear what degree of accuracy is required in the design of a surrogate for it to replicate the hydrodynamic performance of the prototype organism. For example, Aberle and Järvelä (2013) and Boothroyd *et al.* (2016) concluded that the presence of leaves in riparian vegetation has a considerable impact on both the drag force experienced by vegetation and the way in which it modifies the flow characteristics. At a smaller scale, Albayrak *et al.* (2012) reported that roughness, shape, and serration (and their combination) can alter considerably the drag force exerted by a turbulent flow on a leaf replica (i.e. its drag coefficient). Since the hydrodynamic performance of any organism is characterised by the elements of which it is composed, we believe that investigation of vegetation hydrodynamics should start from the simplest element, i.e. a leaf or blade.

In the present study we assess the effect of designing vegetation surrogates using vegetation main dimensions and morphological characteristics, and mechanical properties, but without taking into account other morphological features, by comparing the hydrodynamic performance of seaweed blades of the species *Saccharina latissima* and those of their plastic surrogates. *S. latissima* was chosen because of its relatively simple morphology and its potential application in seaweed farming (Vettori 2016). Blade surrogates were designed and manufactured according to a similarity theory described in Vettori and Nikora (2017b). Hydrodynamic performance of individual test samples at a range of hydraulic conditions was assessed in a laboratory flume by measuring flow velocities upstream and downstream from the samples, the drag force exerted by the flow on the samples, and their vertical reconfiguration. The interrelations between flow turbulence, fluctuations of the drag force and sample reconfiguration are also examined to shed a light on the mechanisms controlling samples hydrodynamics. Ultimately, we seek to evaluate if the surrogates we designed and manufactured are reliable replicas of live seaweed blades. Stemming from this, we aim to understand what is the degree of accuracy required for the design of seaweed blade surrogates and

vegetation surrogates in general. We also note that the data used in this study were used in Vettori and Nikora (2017b) and Vettori and Nikora (unpublished) to characterise the hydrodynamics of artificial surrogates and seaweed blades, respectively. Section 2 contains a description of the test samples (i.e. seaweed blades and their artificial surrogates), instrumentation, and data processing techniques used in this study. In Sect. 2 we also compare the morphology and the mechanical properties of test samples. In Sect. 3 results and findings of the study are reported with focus on the drag force acting on the test samples, their reconfiguration, their effects on the downstream flow characteristics, and the speed of propagation of oscillations along them. In Sect. 4 we discuss the results of the study and provide a comprehensive assessment of how well our seaweed blade surrogates replicate the performance of live seaweed blades.

2 Materials and Methods

2.1 Test samples

Artificial surrogates of blades of *S. latissima* were designed based on a similarity theory for seaweed blades described in Vettori and Nikora (2017b) which maintains geometrical, kinetic, and dynamic similarities by keeping the blade Reynolds number ($\mathrm{Re}_l = U_{up}l/\nu$) and the Cauchy number ($\mathrm{C}_y = \rho U_{up}^2 l^3/(E_s t^3)$) identical for both the prototypes and the surrogates. Data of morphological characteristics and mechanical properties of seaweed blades available in the literature (e.g. Buck and Buchholz 2005, Boller and Carrington 2007, Spurkland and Iken 2012) were used for the design of surrogates. Since previous studies report only mean values for blade width (b) and thickness (t), surrogates were manufactured with constant width and thickness, the only exceptions being the blade ends, which were rounded to replicate a natural shape (Fig. 1). It is also noted that Boller and Carrington (2007) report an estimate of Young's modulus at tension rather than bending; nevertheless, their estimate was used as reference due to the lack of alternative information. Nine surrogates with a range of morphological characteristics and mechanical properties were manufactured using low density polyethylene sheetings and tested in 2014, prior to examining live seaweed blades. We provide a full account of the similarity considerations for seaweed blades and the design and manufacture of the surrogates in Vettori and Nikora (2017b). However, bear in mind that the scale ratios obtained from similarity considerations are 1:5 for geometrical parameters, 1:1 for mass density, and 25:1 for Young's modulus. These target scale ratios were respected approximately in the surrogates due to technical and material limitations. A summary of surrogates' characteristics is reported in Table 1.

Each surrogate was tested at seven flow scenarios described in Table 2.

About 80 samples of *S. latissima* were collected from Loch Fyne (Scotland) on the 10th of February 2015 (coordinates of the site: 56.08 N and 5.28 W, for further details see Vettori and Nikora 2017a). Seaweed samples were kept in seawater during transport to the University of Aberdeen. Within 12 hours from collection samples were placed in a 125 l outdoor tank filled with seawater and featuring a custom-made aeration system. Samples collected were sorted into five groups depending on the length of their blade (see Vettori 2016); from each group three blades as similar as possible in length and width were selected and used in flume experiments (Table 1). Since flume experiments were conducted in freshwater, which can cause a variation in seaweed mechanical properties (Vettori and Nikora, unpublished), each blade was tested in a flow scenario and subsequently discarded. For each group a blade was tested at flow scenario 'Run1', one at 'Run 4', and one at 'Run 7'. Only these flow scenarios were used for live seaweed blades due to time and seaweed supply limitations. Flume experiments with seaweed blades were conducted within 14 days from samples collection. When a sample was selected, its holdfasts and most of its stipe were removed (a part of the stipe was maintained to attach the blade to the Drag Measurement Device, see text below in *Experimental set-up*) so that only the blade was effectively tested. Only blades with no clear signs of deterioration were employed.

Morphologies of seaweed blades and surrogates are compared qualitatively and quantitatively in Fig. 1 by superimposing the contour of a surrogate on the photo of a blade and exhibiting the wetted area of test samples as a function of their length, respectively. From Fig. 1 it is evident that both the shape and the surface area of surrogates differ, to some degree, from those of live blades used in flume experiments. As we discussed in Vettori and Nikora (2017a), this variation appears to be due to the different environmental (e.g. hydraulic) conditions to which seaweeds had been exposed and adapted. Seaweed samples studied by Buck and Buchholz (2005), which were used as prototypes for our surrogates, were collected from exposed site, while live blades considered in the present study were collected from a relatively sheltered site (Vettori and Nikora 2017a).

2.2 Experimental set-up

The hydrodynamic performance of test samples was evaluated by conducting experiments in a12.5 m long, 0.3 m wide, and 0.45 m deep tilting recirculating flume in the Fluid Mechanics Laboratory of the University of Aberdeen (Scotland, UK). Experiments were carried out at quasi-uniform flow conditions with a water depth (H_w) set to 0.3 m, test samples were located in the flume central section and 0.22 m above the

flume bed to minimise the effects of boundaries. The drag force experienced by a test sample was measured at 200 Hz using a Drag Measurement Device (DMD) which included a load cell featuring a Wheatstone bridge (the instrument is described in Vettori and Nikora 2017b). The flow velocities upstream and downstream of a test sample were measured at 100 Hz using two *Vectrino+* (Nortek AS, Rud, Norway) Acoustic Doppler Velocimeters (ADVs) whose sampling volumes were located at the same height of the test sample and 0.2 m upstream of its clamped end and 0.1 m downstream of its free end, respectively. Test sample vertical reconfiguration was monitored by analysing videos recorded with a Full HD digital camera (HD HMX-R10BP, Samsung, Seoul, South Korea) at 25 Hz. The camera was located on the side of a flume glass wall so that the video provided a complete side-view of the test sample at all times during an experiment. An overview of the experimental setup is displayed in Fig. 2. Synchronisation of the ADVs and the DMD was achieved in every experiment via a voltage output trigger. Videos of live seaweed blades were synchronised with ADVs and DMD during video post-processing.

Experiments with blade surrogates had a duration of 10 minutes; a comprehensive description of the experimental setup can be found in Vettori and Nikora (2017b). Experiments with live seaweed blades lasted for about 80 minutes, however, we focus our analysis on the last 10-minute window. This was done because the drag force experienced by seaweed blades decreased considerably for the first 30-50 minutes of experiments (Vettori and Nikora unpublished). The last 10-minutes window of experiments was chosen for consistency with experiments with blade surrogates and because live blades appeared to have completed their adaptation to experimental conditions, thus the measured signals are considered to be stationary in a statistical sense.

2.3 Data processing and analysis

Data of drag force were filtered with an anti-aliasing low-pass FIR filter during conversion from analogue to digital signal. This introduced a delay of 0.025 s in the data that is assumed as negligible for further analysis. Due to the high sensitivity of the load cells used in the DMD, mechanical vibrations inherent to the facility and DMD contaminated the measured drag force signal at frequencies higher than 5 Hz. For live seaweed blades the statistical moments of the drag force are not affected significantly by these vibrations, however the drag spectra S_d exhibit some narrow peaks at frequencies higher than 5 Hz (Fig. 5a). Note that these peaks were not removed during data processing to preserve S_d original characteristics. Conversely, the drag force signal of

blade surrogates was processed with an additional low-pass FIR filter (cut-off frequency set to 4.5 Hz) to cut off the frequencies affected by external vibrations. This second filtering was required because the drag variance σ^2_d would have been significantly biased otherwise and is the reason for which S_d for surrogates stops at 4.5 Hz (Fig. 5a). The filtered signal was then used to calculate all relevant statistical quantities for drag force.

Data collected with the ADVs were despiked using the modified phase-space threshold method (Goring and Nikora 2002, Parsheh *et al.* 2010) and removed points were replaced using the last good value approach.

Vertical positions of a test sample during experiments were extracted from videos using the Canny edge detector algorithm (Canny, 1986) by using MATLAB® image processing tool. Vertical positions were obtained for a number of cross-sections along the test sample (for additional details of the procedure see Vettori and Nikora 2017b), but we focus our analysis mainly on the free end of the test sample, as this position is the most representative for the sample as a whole. From the signal of blade vertical position z_b thus obtained, the vertical velocity w_b of a blade was estimated as a derivative of z_b in time. Applying a cross-correlation technique to the vertical positions of two cross-sections along a test sample, we also estimated the propagation velocity of oscillations of blades (for a more comprehensive description see Vettori 2016).

Further, we estimated the location of the resultant drag force with the same method applied by Siniscalchi and Nikora (2012). This variable can provide additional information on the mechanisms adopted by a blade to reduce drag. The method is based on cross-correlation functions between the flow longitudinal velocities upstream u_{up} and downstream u_{ds} of a test sample and the drag force d experienced by the sample. By identifying the maximum in the cross-correlation function between d and either u_{up} or u_{ds}, the time delay $\Delta\tau$ between the two signals was estimated. From it and knowing the bulk convection velocity U_c, which can be assumed to be equal to the mean approach velocity in front of a test sample U_{up} in the cases investigated (i.e. Taylor's hypothesis of frozen turbulence was found to be valid, see Vettori 2016), the distances between two signal sources (Fig. 2) were estimated, i.e.:

$$L_{up} = U_c \, \Delta\tau_{u\text{-}d} \quad (1)$$

$$L_{ds} = U_c \, \Delta\tau_{d\text{-}u} \quad (2)$$

where L_{up} and L_{ds} are the distances between the sources of the signals u_{up} and d, and d and u_{ds}, respectively, and $\Delta\tau_{u\text{-}d}$ and $\Delta\tau_{d\text{-}u}$ are the time delays between u_{up} and d, and d and

u_{ds}, respectively. From these parameters, it is also possible to compare the validity of the estimate by comparing the distance between two ADVs with the sum of L_{up} and L_{ds}. While the distance of the resultant drag force from the sample clamped end D_{res} is estimated as the difference between L_{up} and the distance between the upstream ADV and the part of the DMD holding the test sample (i.e. 0.2 m) (Fig. 2).

3 Results

Since seaweed blades and their surrogates are characterised by different sizes, to conduct a valid comparison of test samples hydrodynamic performance we make use of normalised parameters and functions such as the drag coefficient C_d, normalised power spectra (i.e. S/σ^2), and squared gain factors $|H|^2$.

3.1 Drag force

A non-dimensional parameter that is used to assess the efficiency of reconfiguration mechanisms in reducing the mean drag force F_d as the mean flow velocity increases ($F_d \propto U_{up}^{2+E}$) is Vogel's exponent E, which was introduced by Vogel (1994). The ranges of values of E for seaweed blades and their surrogates are similar, varying from -0.6 to -0.2 and from -0.6 to 0.2, respectively. Most surrogates are characterised by negative Vogel's exponent, but for the two longest samples (i.e. 'L8', 'L9'). The drag coefficient of artificial surrogates is biased low compared to that of the seaweed blades used in the experiments (Fig. 3). The difference in the domain of the blade Reynolds number R_l (Fig. 3a) is almost null for R_l lower than 2×10^4, but surrogates appear to have a C_d which is approximately 50% lower than that of seaweed blades for higher values of R_l. The divergence in the drag coefficient is more pronounced in the domain of the Cauchy number C_y (Fig. 3b) where, partially due to variations of E_s and t from target values obtained from similarity consideration, C_d of surrogates does not overlap the range of C_d of seaweed blades. Values of C_d of surrogates as a function of C_y are from three to five times lower than those of seaweed blades. This considerable difference is likely to be related to the morphological differences between test samples.

Fluctuations of the drag force are assessed using the spectrum of drag S_d normalised by the drag variance σ^2_d (Fig. 4a) and the ordinary coherence function between the longitudinal flow velocity upstream of the sample and the drag force $\gamma^2_{u\text{-}d}$ (Fig. 4b). The similarity in the spectra of drag force is evident up to 4 Hz, at which frequency the spectra for surrogates are cut off. All cases are well described by a '-1' scaling region at frequencies lower than about 0.1-0.2 Hz and a '-5/2' scaling region between 0.1-0.2 Hz and 5-10 Hz. Exceptions are represented by surrogates 'L1' and 'L2', whose spectrum has a constant slope that follows a '-1' power law; this peculiarity

is discussed comprehensively in Vettori and Nikora (2017b). Also the ordinary coherence function $\gamma^2_{u\text{-}d}$ is similar for seaweed blades and surrogates, however $\gamma^2_{u\text{-}d}$ for seaweed blades is shifted at higher values of the ratio of seaweed blade length l to eddy length scale U_{up}/f compared to that of surrogates. For surrogates $\gamma^2_{u\text{-}d}$ is maximum at $fl/U_{up} < 0.2$, while for seaweed blades the maximum value is at $fl/U_{up} < 2$.

3.2 Reconfiguration

The bulk statistics of vertical position and velocity of surrogates are in general agreement with those of seaweed blades. For example, the mean vertical position is almost constant along the test samples (i.e. samples are streamlined with the main flow) and the mean vertical velocity is null. Moreover, the standard deviation of vertical position σ_{zb} increases quasi-linearly along the samples. The main difference between surrogates and live seaweed blades lies in the magnitude of σ_{zb}, which is one order of magnitude higher for seaweed blades even when comparing test samples of similar length. As described in Vettori and Nikora (2017b, unpublished), for both seaweed blades and their surrogates the test sample free end is used as a descriptor of the whole body for additional statistical analysis.

The spectra S_{wb} of vertical velocity of test samples (i.e. of their free end) are shown in Fig. 5a normalised by σ^2_{wb} and as a function of the ratio of the sample length to eddy length scale. For both seaweed blades and surrogates S_{wb}/σ^2_{wb} show the same patterns, with the spectra collapsing in the same family of curves (Fig. 5a). Therefore, the dynamics of test samples appear to be similar regardless of the nature of samples. However, for live seaweed blades the normalised spectra have a wider region of maximum (i.e. more broadbanded), hinting that the dynamics of live seaweed blades is characterised by movements with a range of wavelengths broader than that for surrogates.

Analysis of the square gain factor ($|H|^2 = S_{wb}/S_{w\text{-}up}$) of the upstream vertical velocity and test sample vertical velocity (Fig. 5b) provides further indication on the dynamics of test samples. Considering the general trend, live seaweed blades and their surrogates perform similarly, but two differences are noticeable: (1) neglecting the peaks at high frequencies that are associated with the effect of vortex shedding on sample's free end, $|H|^2$ have a narrow peak at fl/U_{up} around 0.3-2 for surrogates, while the region of maximum for seaweed blades is broader, going from 0.2 to 10; (2) the magnitude of $|H|^2$ for surrogates is considerably higher than that for seaweed blades at most frequencies. These results indicate that: (i) the turbulent structures that drive test samples (regardless of their nature) most efficiently are those with length scales similar to l; (ii) surrogates are 'specialist', interacting mainly with turbulent structures with

length scale between 0.5l and 3l (i.e. fl/U_{up} from 0.3 to 2) , while seaweed blades interact with a broader range of turbulent structures between 0.1l and 5l; and (iii) seaweed blades are able to dampen flow driving forces more effectively than surrogates, likely due to their bigger wetted surface area and more sophisticated morphological features.

3.3 Effects on flow characteristics

Both seaweed blades and artificial surrogates were found to reduce the mean flow velocity and enhance turbulence downstream of them (Vettori and Nikora 2017b, unpublished). The decay of these effects was examined by looking at the wake evolution downstream of surrogates in Vettori and Nikora (2017b) but was not investigated for seaweed blades due to time constraints. A vortex shedding phenomenon was identified downstream of test samples for both seaweed blades and surrogates at low mean flow velocity (i.e. flow scenarios 'Run 1', 'Run 2' and 'Run 3').

Among flow velocity components, the longitudinal component u is the most affected by test samples followed by w, while v appears to be unindicative. Using the squared gain factors ($|H|^2 = S_{u\text{-}ds}/S_{u\text{-}up}$ and $|H|^2 = S_{w\text{-}ds}/S_{w\text{-}up}$) of flow velocities upstream and downstream of test samples (Fig. 6) we can compare the length scales of the turbulent structures affected by the samples. It is apparent that live seaweed blades have a more considerable effect on longitudinal velocity than surrogates, while the magnitude of $|H|^2$ for vertical velocity matches. Seaweed blades enhance fluctuations in u by up to 10 times from fl/U_{up} = 5 to 30 (Fig. 6a) or in absolute values between approximately 0.01 m and 0.1 m (Fig. 6b). Surrogates enhance turbulence in a very narrow band with length scales smaller than 0.05 m (Fig. 6b). The effects of test samples on fluctuations in w are similar when analysed as a function of the ratio of sample length to eddy length scale (Fig. 6c), but show a relative divergence when analysed as a function of the wavelength (Fig. 6d). Test samples increase fluctuations in w by up to 5 times at a range of length scales between 0.03l and 0.2l (Fig. 6c). In absolute values the scale ranges characterised by turbulence enhancement for w coincide with those for u (Fig. 6d).

3.4 Propagation of sample oscillations

The propagation velocity V_p of oscillations on test samples is normalised using the mean flow velocity in Fig. 7a, where it is shown as a function of the blade Reynolds number. Regardless of the nature of the test samples, V_p/U_{up} has maximum values at low R_l and tends to unity as R_l increases (Fig. 7a). The magnitude of propagation velocity, however, is slightly different for surrogates and seaweed blades, with V_p/U_{up} biased low for surrogates. This deviation might be related to the different procedures applied in the

video analysis, in which reconfiguration of seaweed blades was assumed to be described by the central part (i.e. centroids) of the blade (see Vettori and Nikora 2017b), potentially underestimating the vertical velocity neglecting the lower and upper edges of the blade. Interestingly, in the domain of the blade Reynolds number the trends shown by V_p/U_{up} are somewhat similar to those of the drag coefficient (Fig. 3a).

3.5 Location of the resultant drag force

The location of the resultant drag force differs considerably between seaweed blades and their surrogates (Fig. 7b). Live seaweed blades are characterised by a D_{res} ranging from 0.4l to 0.6l, an evidence of a uniform contribution to drag force of all blade parts. On the opposite, surrogates display a D_{res} located closer to the clamped end of the sample, between 0.05l and 0.25l in most cases, but with some outliers exceeding 0.3l or equal to 0. This suggests that the upstream part of the surrogates has a major contribution to defining the drag force, while the free end is insignificant. In addition, the resultant drag force for all test samples appear to move downstream as the mean flow velocity increases (Fig. 7b) but is not affected by the length of test samples. The accuracy in the estimation of D_{res} was assessed by comparing the distance between the ADVs with the distance between the signal sources of u_{up} and u_{ds} (Vettori 2016). The error is below 10% in 90% of the cases investigated and never above 30%; moreover, the outliers visible in Fig. 7b are never associated with errors above 10%. This excludes problems with the data analysis procedure, rather hinting at a potential issue during data collection (i.e. imperfect synchronisation) in these cases.

4 Discussion

Results of the present study show that C_d of surrogates is biased low compared to that of live seaweed blades, with a 50% difference the domain of R_l and a more marked difference in the domain of C_y. This divergence is ascribed to the different morphologies of surrogates and seaweed blades whose effect is apparent in Fig. 1 both in terms of sample's shape and wetted surface area. The variation of morphological characteristics encountered in this study is associated with the ability of seaweeds to adapt to the environmental conditions to which they are exposed. This ability is referred to as phenotypic plasticity and is a fundamental property of vegetation (e.g. Schlichting, 1986). We designed our surrogates using data available in the literature (i.e. Buck and Buchholz 2005, Spurkland and Iken 2012) that referred to seaweeds grown at exposed sites. Conversely, live seaweed samples use in our study were collected from a sheltered location (Vettori and Nikora 2017a). In terms of mechanical properties, the mass density ρ_s of surrogates is similar to that of seaweed blades (as per target value), but their

Young's modulus at bending E_s is usually higher than the target value obtained from the 25:1 scale ratio (Table 1). This variation, however, should not impact the results significantly, surrogates with E_s closer to the target value not performing more consistently with seaweed blades than other surrogates. Our results, therefore, indicate that C_y as defined in Section 2.1 is not an appropriate adimensional parameter for describing the hydrodynamic performance of seaweed blades. In order to be used on vegetation with relatively complex morphologies, C_y should be either modified in such a way to incorporate additional information (e.g. the roughness of a blade) or applied individually to different parts of an organism (e.g. stems, leaves/blades).

The effect of sample morphology is apparent also in the analyses of test sample dynamics and of the effects of test sample on the flow characteristics. The dynamics of surrogates are controlled by turbulent structures within a narrow range of spatial scale, while the dynamics of seaweed blades are affected by a wider range of eddies. In Fig. 4b $\gamma^2_{u\text{-}d}$ characterises the efficiency with which fluctuations in u_{up} generate fluctuations in d: turbulent structures with length scales greater than $0.5l$ are very efficient at causing drag fluctuations in seaweed blades, while the range of length scales is reduced to values greater than $5l$ for surrogates. Smaller scale eddies are more effective on seaweed blades likely due to their sophisticated morphology (with ruffled edges and bullations). Test sample dynamics is further examined in Fig. 5 focusing on the vertical velocity of test sample's free end. Reconfiguration of test samples is the result of oscillations with a range of wavelengths defined as fl/U_{up} = 0.2 - 10 for seaweed blades and fl/U_{up} = 0.3 – 2 for surrogates (Fig. 5a). Similar ranges of spatial scales are evinced for the turbulent structures that drive sample dynamics most efficiently (Fig. 5b). We also note that the peaks present at high frequencies in Fig. 5b are not associated with a real mechanism, rather than that they are an artefact generated by vortices shed by test sample's free end at low flow velocities. These vortices can feed test sample dynamics by inducing vibrations within a well-defined frequency range. These vibrations are referred to as vortex induced vibrations in the study of flow-structure interactions and are self-powered, meaning that the same vibrations of the free end induced by the aforementioned vortices contribute to generating vortices in the wake (for a comprehensive description of this phenomenon, see Naudascher and Rockwell 2005). Further, the effects of test samples on fluctuations in u are enhanced considerably in the case of seaweed blades, both in terms of magnitude and range of spatial scales. This is not related with the size of the samples, as surrogates were as long as seaweed blades (or with compatible wetted surface area) in a number of cases, but appears to be due to the complex morphological nature of seaweed blades, similarly to what discussed for the drag force and reconfiguration of test samples.

Even though surrogates do not fully replicate live seaweed blades broadbanded interactions with the flow, they simulate successfully many aspects of seaweed blade hydrodynamics. First, the trend of C_d in the domain of R_l is the same for seaweed blades and their surrogates, similar to that of a flat plate parallel to the flow (Vettori and Nikora 2017b). Second, spectral analysis of drag force and sample vertical velocity show a number of similarities between seaweed blades and their surrogates: (i) for both types of samples S_d is well described by two 'universal' scaling regions (i.e. -1 and -5/2 at a log-log scale), reflecting passive and active interactions between a sample and the flow (Vettori and Nikora 2017b); (ii) their S_{wb} are very similar, with most reconfiguration associated with oscillations with wavelengths similar to sample length l; and (iii) turbulent structures with length scales similar to l are the most efficient in driving sample reconfiguration (Fig. 5b). Third, the effects of test samples on the fluctuations in w are approximately independent of the nature of the sample (Fig. 6c-d), and the normalised propagation velocity of oscillations V_p/U_{up} shows common characteristics for seaweed blades and their surrogates (Fig. 7a). The estimated resultant drag force is located at the centre of a sample for live seaweed blades, while it close to the clamped end for surrogates. The direction of this difference is unexpected, as the stretched droplet shape of live blades (Vettori and Nikora 2017a) would suggest that the upstream part of a blade is the main contributor to drag force. Thus, the design of seaweed blades appears to grant them a more 'balanced' design compared to that of our surrogates. The reasons for this difference and potential consequences on seaweed survival strategy are uncertain.

The results of this study evince that accounting for morphological macro-features such as bullations, ruffles and overall shape is required when designing and manufacturing artificial seaweed surrogates and for replicating seaweeds hydrodynamic performance. This type of approach was adopted by Rominger and Nepf (2014) and Fryer *et al.* (2015) for examining the effects of longitudinal corrugations on the drag force and mass transfer in surrogates of seaweed blades and should be applied more widely. This issue may appear of relatively small importance for bending plants (*sensu* Nikora, 2010) for which the contribution of friction drag is much lower than that of pressure drag. Nevertheless, as demonstrated by Aberle and Järvelä (2013), even riparian vegetation, which presents notorious examples of bending plants, cannot be replicated appropriately if leaves are not taken into account. Furthermore, the drag force exerted by the flow on leaves is dependent upon their morphological characteristics and mechanical properties as concluded by Albayrak *et al.* (2012). In particular Albayrak *et al.* found that an elliptic shape (similar to the shape of live seaweed blades used in the present study) is associated with higher C_d than a rectangular shape (more similar to the

shape of our surogates) for low values of flexural rigidity. Moreover, the presence of roughness elements, such as bullations on seaweed blades, causes an increase in C_d for a leaf/blade. It follows that an accurate and detailed description of morphological characteristics of leaves/blades is of primary importance for achieving an accurate characterisation of the drag force acting on vegetation.

In conclusion, it is critical that we apply a more rigorous approach to the design and manufacturing of vegetation surrogates. Even though in this study we have not examined seaweed blade morphology in detail, our findings suggest that intraspecies morphological variation may play an important role in determining the drag force experienced by an organism. Hence, organisms of the same species growing at different sites and with similar main dimensions (e.g. length, mean width, wetted surface area) may experience drag forces significantly different from each other depending on the environmental factors that have affected their growth. Regarding this matter, we would also like to stress two points: (i) the lack of information of vegetation morphology, particularly for freshwater aquatic species and riparian species, limits our ability to investigate flow-vegetation interactions comprehensively; and (ii) plant allometry (see Niklas 1994) may contain key tools to help us incorporating intraspecies morphological variation in the study of flow-vegetation interactions. Finally, we note that it is currently unclear how vegetation morphological macro-features affect the drag force at a canopy or reach scale (i.e. in those applications in which vegetation is considered as roughness element on the bed of an open channel). Exploratory research in this area is required for providing us with the knowledge and tools for developing mathematical and physical models that are appropriate replicas of field conditions.

5 Conclusions

This paper presents a thorough comparison of the hydrodynamic performance of live seaweed blades of the species *S. latissima* and their surrogates designed basing on similarity considerations. The hydrodynamics of test samples were assessed using data collected during flume experiments featuring synchronised measurements of flow velocities upstream and downstream of test samples, and their drag force and vertical reconfiguration. Surrogates were found to successfully reproduce many aspects of live seaweed blade hydrodynamics and the same controlling mechanisms were identified for live seaweed blades and surrogates. Nevertheless, surrogates did not replicate the performances of live seaweed blades in terms of the drag coefficient and were more selective than live seaweed blades about the range of turbulence structures (i.e. their length scales) characterising their hydrodynamics. The findings of this study indicate that a high degree of accuracy is require in the design of artificial surrogates for

replicating the hydrodynamic performance of vegetation. Macro-features present on the surface of blades have a primary role in determining the drag force exerted on them. Therefore, these often-overlooked morphological features should not be neglected on the design of vegetation surrogates.

Acknowledgements

The authors gratefully acknowledge the assistance of Elisa Bozzolan, Euan Judd, Henry Lecallet, and Olivia McCabe in collecting data sets used in this publication. The authors also thank Stuart Cameron and Euan Judd for support in developing video analysis routines, David Attwood and Hamish Biggs for their assistance during seaweed collection and transport to the University of Aberdeen, and technicians Roy Gillanders and Benjamin Stratton for meticulous technical support of the experiments.

Funding

The work described in this publication was undertaken during the Ph.D. study of Davide Vettori at the University of Aberdeen funded by a scholarship from the Northern Research Partnership, Scotland.

Notation

A_{wet}	=	wetted surface area (mm^2)
b	=	(mean) width of test sample (mm)
b_{max}	=	maximum width of test sample (mm)
C_d	=	drag coefficient (-)
C_y	=	Cauchy number (-)
d	=	instantaneous drag force (N)
D_{res}	=	distance of the resultant drag force from test sample clamped end (mm)
E	=	Vogel's exponent (-)
E_s	=	elastic Young's modulus of test sample at bending (MPa)
f	=	frequency (Hz)
$\|H\|^2$	=	squared gain factor (-)
H_w	=	water depth (m)
k	=	wavenumber (m^{-1})
l	=	length of test sample (mm)
L	=	distance between two ADVs (mm)
L_{ds}	=	distance between signal sources of d and u_{ds} (mm)
L_{up}	=	distance between signal sources of u_{up} and d (mm)
Q	=	flow rate (m^3s^{-1})
R	=	Reynolds number (-)
R_l	=	blade Reynolds number (-)

S_0	=	flume bed slope (-)
S_d	=	power spectral density function of d (N^2 s)
$S_{u\text{-}ds}$, $S_{w\text{-}ds}$	=	power spectral density function of u_{ds} and w_{ds} (mm^2 s^{-1})
$S_{u\text{-}up}$, $S_{w\text{-}up}$	=	power spectral density function of u_{up} and w_{up} (mm^2 s^{-1})
S_{wb}	=	power spectral density function of w_b (mm^2 s^{-1})
t	=	(mean) thickness of test sample (mm)
t_{max}	=	maximum thickness of test sample (mm)
u, v, w	=	velocity components in the x, y, and z directions (mm s^{-1})
u_{ds}, w_{ds}	=	instantaneous u and w downstream of test sample (mm s^{-1})
u_{up}, w_{up}	=	instantaneous u and w upstream of test sample (mm s^{-1})
U_c	=	bulk convection velocity (mm s^{-1})
U_s	=	cross-sectional averaged flow velocity (m s^{-1})
U_{up}	=	time averaged u_{up} (m s^{-1})
V_p	=	propagation velocity on test sample (m s^{-1})
w_b	=	instantaneous vertical velocity of test sample (mm s^{-1})
z_b	=	instantaneous vertical position of test sample (mm)
$\gamma^2_{u\text{-}d}$	=	ordinary coherence function between u_{up} and d (-)
$\Delta\tau$	=	time delay between two signals (s)
ν	=	water kinetic viscosity (m^2 s^{-1})
ρ	=	mass density of water (kg m^{-3})
ρ_s	=	mass density of test sample (kg m^{-3})
σ^2_d	=	variance of d (N^2)
σ^2_{wb}	=	variance of w_b (mm^2 s^{-2})
σ_{zb}	=	standard deviation of z_b (mm)

References

Aberle, J., Järvelä, J. (2013). Flow resistance of emergent rigid and flexible floodplain vegetation. *Journal of Hydraulic Research, 51(1),* 33-45.

Albayrak, I., Nikora, V., Miler, O., O'Hare, M. (2012). Flow-plant interactions at a leaf scale: effects of leaf shape, serration, roughness and flexural rigidity. *Aquatic Sciences, 74(2),* 267-286.

Boller, M. L., Carrington, E. (2007). Interspecific comparison of hydrodynamic performance and structural properties among intertidal macroalgae. *Journal of Experimental Biology, 210(11),* 1874–1884.

Boothroyd, R. J., Hardy, R. J., Warburton, J., Marjoribanks, T. I. (2016). The importance of accurately representing submerged vegetation morphology in the numerical prediction of complex river flow. *Earth Surface Processes and Landforms, 41(4),* 567-576.

Buck, B. H., Buchholz, C. M. (2005). Response of offshore cultivated *Laminaria saccharina* to hydrodynamic forcing in the North Sea. *Aquaculture, 250(3),* 674–691

de Langre, E. (2008). Effects of wind on plants. *Annual Review of Fluid Mechanics, 40,* 141–168.

Canny, J. (1986). A computational approach to edge detection. *IEEE Transactions on pattern analysis and machine intelligence, 6,* 679–698.

Folkard, A. M. (2005). Hydrodynamics of model Posidonia oceanica patches in shallow water. *Limnology and Oceanography, 50(5),* 1592-1600.

Frostick, L. E., McLelland, S. J., Mercer, T. G. (2011). *Users guide to physical modelling and experimentation: experience of the HYDRALAB network.* Boca Raton: CRC Press.

Fryer, M., Terwagne, D., Reis, P. M., Nepf, H. (2015). Fabrication of flexible blade models from a silicone-based polymer to test the effect of surface corrugations on drag and blade motion. *Limnology and Oceanography: Methods, 13(11),* 630-639.

Ghisalberti, M., Nepf, H. (2005). Mass transport in vegetated shear flows. *Environmental fluid mechanics, 5(6),* 527-551.

Goring, D. G., Nikora, V. I. (2002). Despiking acoustic Doppler velocimeter data. *Journal of Hydraulic Engineering, 128(1),* 117–126.

Johnson, A.S. (2001). Drag, drafting, and mechanical interactions in canopies of the red alga *Chondrus crispus*. *The Biological Bulletin, 201(2),* 126-135.

Kouwen, N., Unny, T. E., Hill, H. M. (1969). Flow retardance in vegetated channels.

Journal of the Irrigation and Drainage Division, 95(2), 329-344.

Kouwen, N., Unny, T. E. (1973). Flexible roughness in open channels. *Journal of the Hydraulics Division, 99*(hy5).

Lightbody, A. F., Nepf, H. M. (2006). Prediction of near-field shear dispersion in an emergent canopy with heterogeneous morphology. *Environmental Fluid Mechanics, 6(5)*, 477-488.

Lucas, J. S., Southgate, P. C. (2012). *Aquaculture: farming aquatic animals and plants*. Hoboken: Wiley-Blackwell.

Naudascher, E., Rockwell, D. (2005). *Flow-induced Vibrations: An Engineering Guide*. New York: Dover Publications Inc.

Nezu, I., Sanjou, M. (2008). Turbulence structure and coherent motion in vegetated canopy open-channel flows. *Journal of Hydro-environment Research, 2(2)*, 62-90.

Niklas, K. J. (1994). *Plant allometry: the scaling of form and process*. Chicago: University of Chicago Press.

Nikora, V. (2010). Hydrodynamics of aquatic ecosystems: an interface between ecology, biomechanics and environmental fluid mechanics. *River Research and Applications 26(4)*, 367–384.

Nikora, N., Nikora, V., O'Donoghue, T. (2013). Velocity profiles in vegetated open-channel flows: combined effects of multiple mechanisms. *Journal of Hydraulic Engineering, 139(10)*, 1021-1032.

Parsheh, M., Sotiropoulos, F., Porte´-Agel, F. (2010). Estimation of power spectra of acoustic-Doppler velocimetry data contaminated with intermittent spikes. *Journal of Hydraulic Engineering, 136(6)*, 368–378.

Rominger, J. T., Nepf, H. M. (2014). Effects of blade flexural rigidity on drag force and mass transfer rates in model blades. *Limnology and Oceanograph, 59(6)*, 2028-2041.

Schlichting, C. D. (1986). The evolution of phenotypic plasticity in plants. *Annual Review of Ecology and Systematics, 17 (1)*, 667-693.

Shumway, R. H., Stoffer, D. S. (2000). *Time series analysis and its applications*. Berlin: Springer.

Siniscalchi, F., Nikora, V. (2012). Flow-plant interactions in open-channel flows: a comparative analysis of five freshwater plant species. *Water Resources Research, 48(5)*.

Siniscalchi, F., Nikora, V. I., Aberle, J. (2012). Plant patch hydrodynamics in streams: Mean flow, turbulence, and drag forces. *Water Resources Research, 48(1)*.

Siniscalchi, F., Nikora, V. (2013). Dynamic reconfiguration of aquatic plants and its interrelations with upstream turbulence and drag forces. *Journal of Hydraulic Research, 51(1),* 46–55.

Spurkland, T., Iken, K. (2012). Seasonal growth patterns of *Saccharina latissima* (Phaeophyceae, Ochrophyta) in a glacially-influenced subarctic estuary. *Phycological Research, 60(4),* 261–275.

Stewart, H.L. (2006). Hydrodynamic consequences of flexural stiffness and buoyancy for seaweeds: a study using physical models. *Journal of Experimental Biology, 209(11),* 2170-2181.

Vettori, D. (2016). *Hydrodynamic performance of seaweed farms: an experimental study at seaweed blade scale* (PhD thesis). University of Aberdeen, Aberdeen, Scotland, UK.

Vettori, D., Nikora, V. (2017a). Morphological and mechanical properties of blades of Saccharina latissima. *Estuarine, Coastal and Shelf Science, 196,* 1–9.

Vettori, D., Nikora, V. (2017b). Flow–seaweed interactions: a laboratory study using blade models. *Environmental Fluid Mechanics.* doi: 10.1007/s10652-017-9556-6

Vogel, S. (1994). *Life in moving fluids: the physical biology of flow*. Princeton: Princeton University Press.

Wilson, C. A. M. E., Stoesser, T., Bates, P. D., Pinzen, A. B. (2003). Open channel flow through different forms of submerged flexible vegetation. *Journal of Hydraulic Engineering, 129(11),* 847-853.

List of tables

List of figures

Table 1 Summary of morphological and mechanical characteristics of seaweed blades and their surrogates. Seaweed blades are ordered by length group and flow scenario, artificial surrogates are ordered by length. Note that values of mass density and bending Young's modulus of seaweed blades are mean values obtained from measurements of about 80 blades (see Vettori and Nikora, 2017). Also note that the maximum and mean values of width and thickness of surrogates are identical because surrogates were designed with a uniform width.

	l (mm)	b (mm)	b_{max} (mm)	t (mm)	t_{max} (mm)	A_{wet} (mm^2)	ρ_s (kg m^{-3})	E_s (MPa)
Seaweeds								
	196	38	62	0.18	0.43	1.4×10^4	1092	3.73
Group 1	160	34	63	0.16	0.47	1.2×10^4	1092	3.73
	205	36	68	0.23	0.42	1.6×10^4	1092	3.73
	275	36	77	0.17	0.65	2.6×10^4	1092	3.73
Group 2	285	39	82	0.20	0.52	2.8×10^4	1092	3.73
	310	36	81	0.21	0.91	3.4×10^4	1092	3.73
	424	47	132	0.23	0.93	6.2×10^4	1092	3.73
Group 3	444	41	134	0.26	0.70	6.2×10^4	1092	3.73
	419	49	124	0.24	0.76	5.4×10^4	1092	3.73
	519	45	181	0.24	0.83	1.1×10^5	1092	3.73
Group 4	548	54	174	0.41	0.82	1.1×10^5	1092	3.73
	516	49	17	0.36	1.54	1.3×10^5	1092	3.73
	570	74	127	0.25	0.85	7.2×10^4	1092	3.73
Group 5	599	76	143	0.29	1.82	9.8×10^4	1092	3.73
	601	69	118	0.28	1.21	8.2×10^4	1092	3.73
Surrogates								
L1	70	6	6	0.07	0.07	4.0×10^2	1059	240
L2	90	7	7	0.12	0.12	6.3×10^2	935	205
L3	100	8	8	0.10	0.10	7.6×10^2	819	319
L4	120	9	9	0.12	0.12	1.1×10^3	935	205
L5	190	10	10	0.12	0.12	2.0×10^3	935	205
L6	210	11	11	0.21	0.21	2.5×10^3	856	78
L7	280	15	15	0.28	0.28	4.1×10^3	992	209
L8	290	15	15	0.12	0.12	4.3×10^3	935	205
L9	390	26	26	0.12	0.12	1.0×10^4	935	205

Table 2 Description of hydraulic conditions of experiments.

Flow scenario	S_0	Q ($m^3 s^{-1}$)	H_w (m)	U_{up} ($m s^{-1}$)	U_s ($m s^{-1}$)	$R = U_{up}H_w/\nu$
Run 1	1:1000	7.0×10^{-3}	0.3	0.10	0.09	27,000
Run 2	1:1000	11.8×10^{-3}	0.3	0.18	0.16	48,000
Run 3	1:1000	16.6×10^{-3}	0.3	0.26	0.22	66,000
Run 4	1:1000	21.5×10^{-3}	0.3	0.33	0.29	87,000
Run 5	1:1000	26.4×10^{-3}	0.3	0.40	0.35	105,000
Run 6	1:500	31.2×10^{-3}	0.3	0.47	0.42	126,000
Run 7	1:500	36.0×10^{-3}	0.3	0.55	0.48	144,000

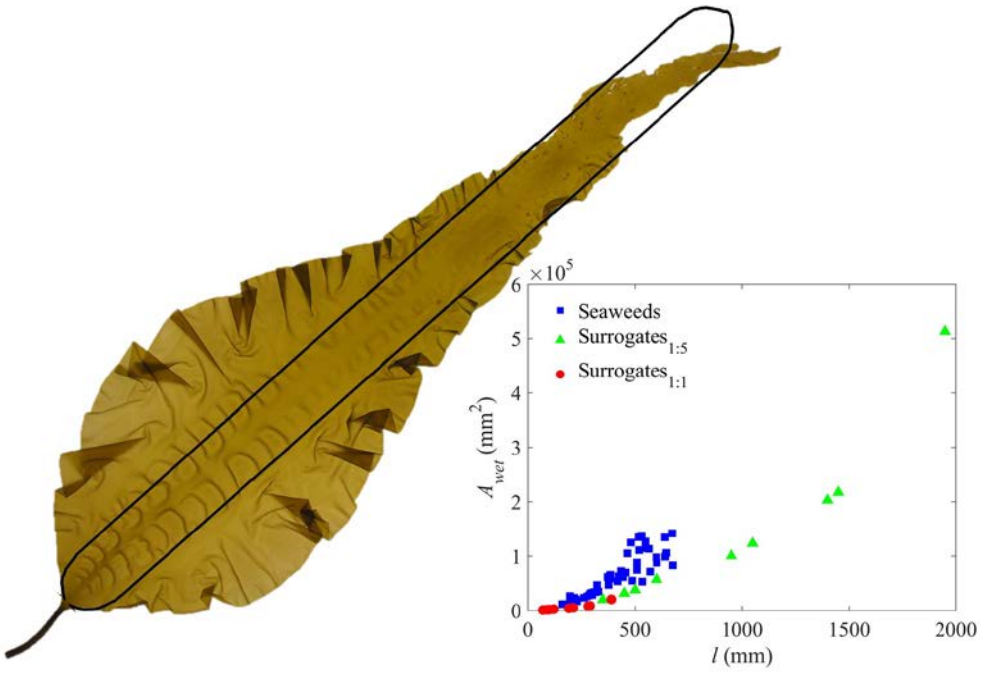

Figure 1 A seaweed blade (background) and a seaweed blade surrogate (black contour). The surrogate is shown at the scale 1:1. Comparison of wetted surface area of seaweed blades and their surrogates, values of surrogates at the scales 1:5 and 1:1 are reported (inset).

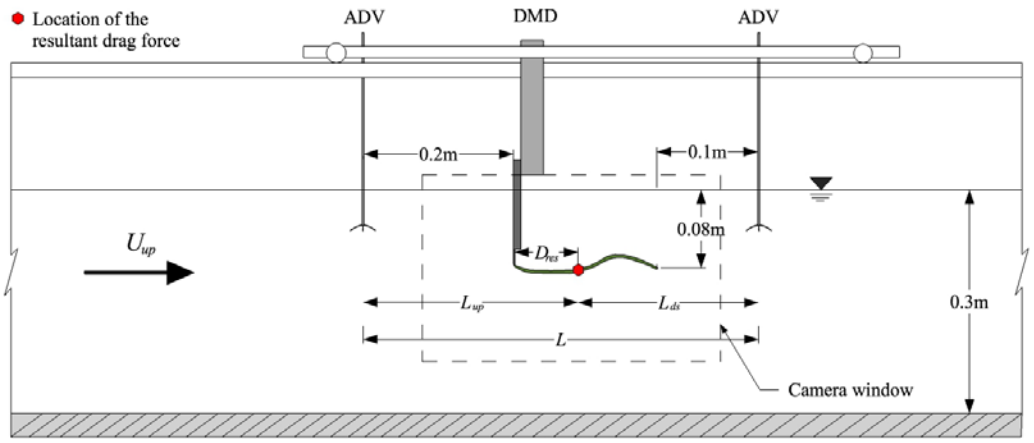

Figure 2 Side view of the experimental setup for assessing the hydrodynamic performance of test samples including parameters used in the estimation of the location of the resultant drag force.

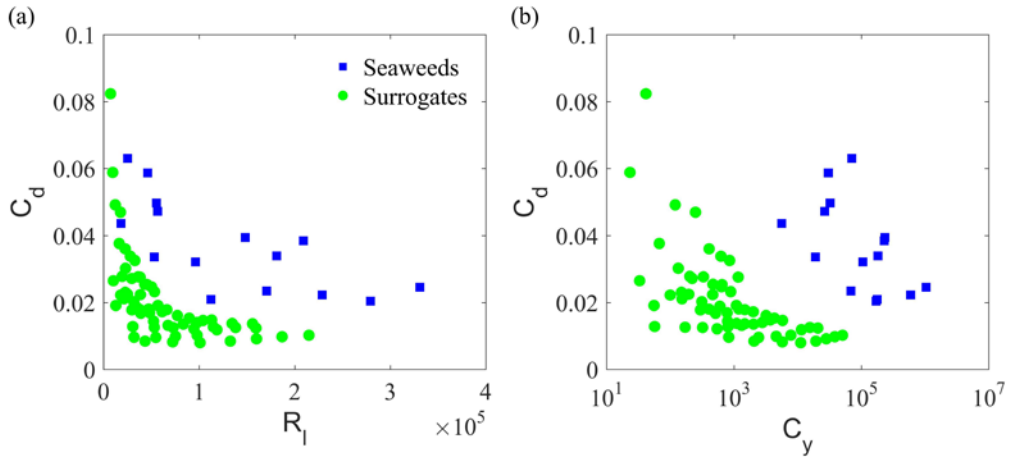

Figure 3 Drag coefficient of test samples as a function of: (a) the blade Reynolds number and, (b) the Cauchy number.

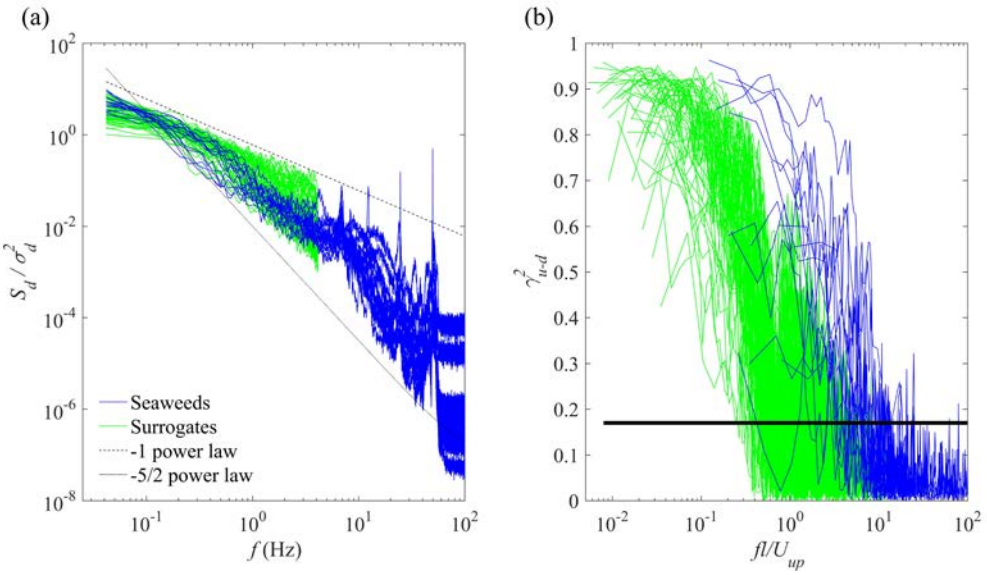

Figure 4 (a) Spectrum of the drag force experienced by test samples normalised by drag variance. (b) Ordinary coherence function between u_{up} and d; the thick horizontal line represents 1% significance level of the coherence function computed according to Shumway and Stoffer (2000).

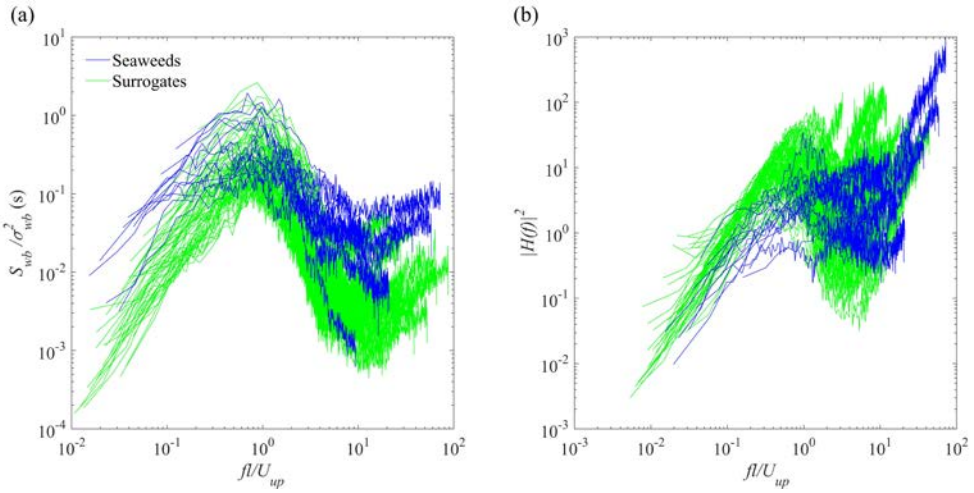

Figure 5 (a) Spectrum of the vertical velocity of test samples normalised by vertical velocity variance as a function of the ratio of sample length to eddy length scale. (b) Squared gain factor of the flow vertical velocity upstream of the test sample and sample's free end vertical velocity as a function of the ratio of sample length to eddy length scale.

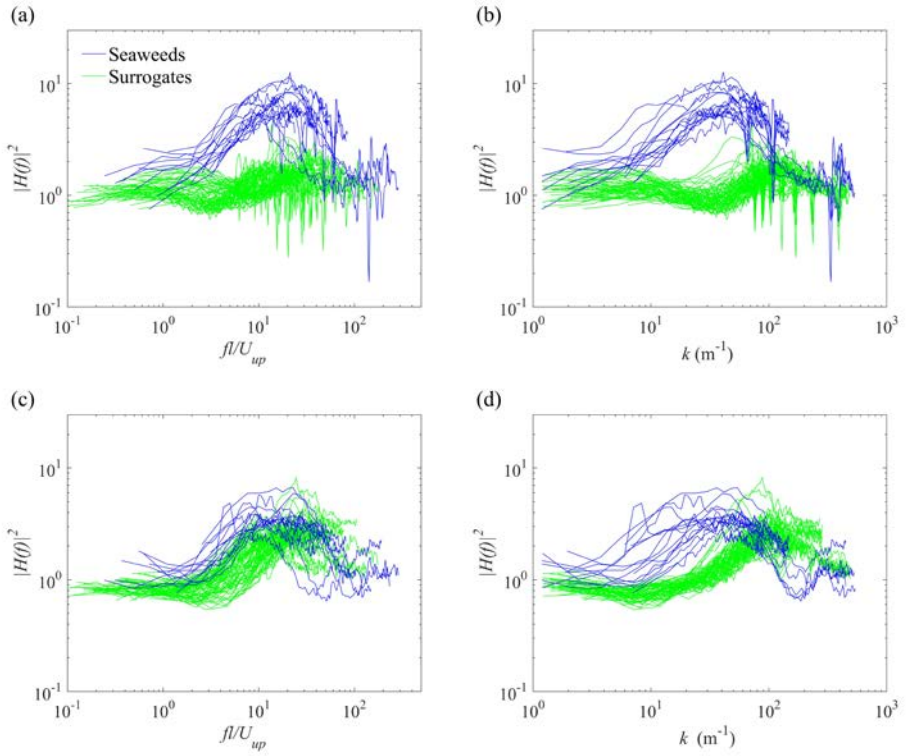

Figure 6 Effects of test samples on flow characteristics assessed via squared gain factors of flow velocity components *u* (a-b) and *w* (c-d) upstream and downstream of the test samples: (a, c) squared gain factor is shown as a function of the ratio of sample length to eddy length scale; and (b, d) squared gain factor is shown as a function of the wavenumber.

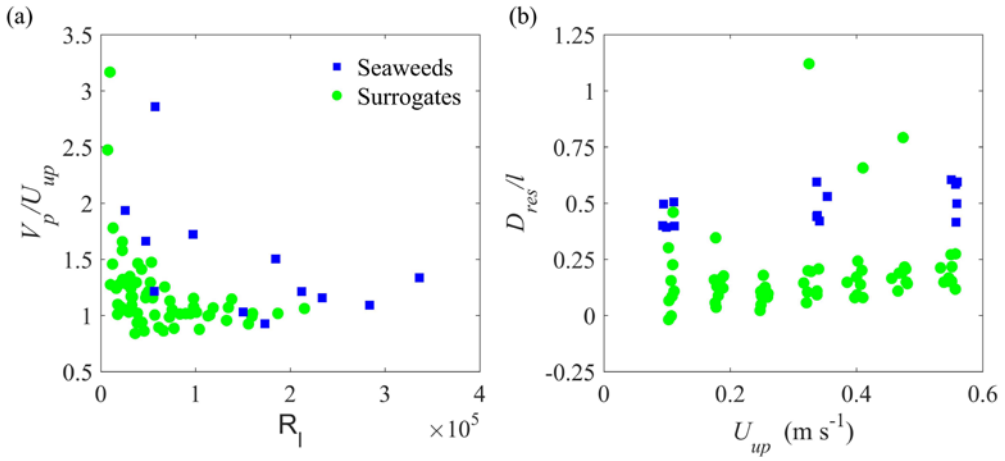

Figure 7 (a) Estimates of the propagation velocity normalised by the mean approach velocity in front of a test sample as a function of the blade Reynold number. (b) Distance of the location of the resultant drag force from the sample clamped end normalised by sample length as a function of the mean approach velocity in front of a test sample.